Inorganica Chimica Acta 446 (2016) 24–31

Contents lists available at ScienceDirect

Inorganica Chimica Acta

journal homepage: www.elsevier.com/locate/ica

Modifying a composite based on silica molecular sieve and a Ru(II)-based probe with Fe_3O_4 particles: Construction and oxygen sensing performance

Chen Lin, Sun Shuai, Li Jia, Fang Zhigang *

School of Chemical Engineering, University of Science and Technology Liaoning, Anshan 114051, China

ARTICLE INFO

Article history:
Received 31 January 2016
Received in revised form 29 February 2016
Accepted 29 February 2016
Available online 5 March 2016

Keywords:
Fe_3O_4 core
O_2 sensing
Ru(II) complex
Linear response
Stern–Volmer plot

ABSTRACT

This paper reported a composite based on silica molecular sieve MCM-41 and a Ru(II)-based probe which was further functionalized with magnetic Fe_3O_4 so that site-specific guiding could be achieved. A core–shell structure was applied in this composite, with Fe_3O_4 as core and MCM-41 as shell, respectively. By means of electron microscope images, XRD analysis, IR spectra, N_2 adsorption/desorption measurement and thermal degradation analysis, this composite was analyzed and confirmed. Emission monitoring of this composite under various O_2 concentrations suggested that its emission was quenchable by O_2 through a dynamic mechanism with good stability. Sensitivity of 11.5 and short response time of 10 s were obtained with a linear working plot.

1. Introduction

Being a life-supporting gas, molecular O_2 has been considered important. Its quantification is consequently highly focused in various fields such as chemical industry, environmental protection and food processing/preservation [1,2]. As a novel quantification method, optical sensing has been highly proposed among the numerous candidates owing to its advantages of instant response, simple operational procedure, requiring no sophisticated apparatus and low cost. In addition, optical signals are free of electromagnetic interference, which makes long-distance on-line monitoring and in-field detection possible [3–6]. After comparing performance between sensing systems based on pure materials and those based on organic–inorganic composite materials, composite sensing systems are found better since they gather virtues of each component and well preserve them, resulting in various feature combinations to meet practical application [7–12].

In this case, inorganic component of a composite system usually serves as supporting matrix owing to its good mechanical strength and stability. To realize desired performance, some criteria should be met by such supporting matrix, including high diffusion coefficient, uniform microenvironment and compatibility with sensing probe. Among the numerous candidates for supporting matrix, a silica molecular sieve MCM-41 has been frequently suggested in virtue of its highly ordered tunnels which satisfy criteria for an ideal supporting matrix well [11,12].

While, the organic component in a composite material is usually applied as sensing probe owing to its good optoelectronic features [10–17]. Aiming at complete and fast sensing with analyte, long lifetime and broad distribution of excited electrons are expected. It appears that luminescent metal complexes are promising ones. Their emission is originated from triplet metal-to-ligand-charge-transfer (MLCT) excited state and generally has a long-lived lifetime of microseconds. Generally, excited electrons are localized on conjugation chain of ligands and thus can be readily spread, satisfying above demands.

To properly combine organic and inorganic components and preserve their features, a number of hybrid structures have been proposed [11–18]. Core–shell structure has been considered promising owing to its simple construction route, excellent holding and preservation of components [15–18]. There is only one issue that fails to be counted for practical applications, which is site-specific guiding. Guided by above consideration, we intend to modify an optical sensing system with magnetic Fe_3O_4 so that site-specific oxygen sensing can be achieved. Its design strategy and detailed construction route are shown as Scheme 1 (see Supporting information for a detailed explanation on design strategy of Ru-Phen@MCM-41@Fe_3O_4).

* Corresponding author. Tel.: +86 0412 5929637.
E-mail address: anshan_chenlin1@163.com (L. Chen).

http://dx.doi.org/10.1016/j.ica.2016.02.061
0020-1693/

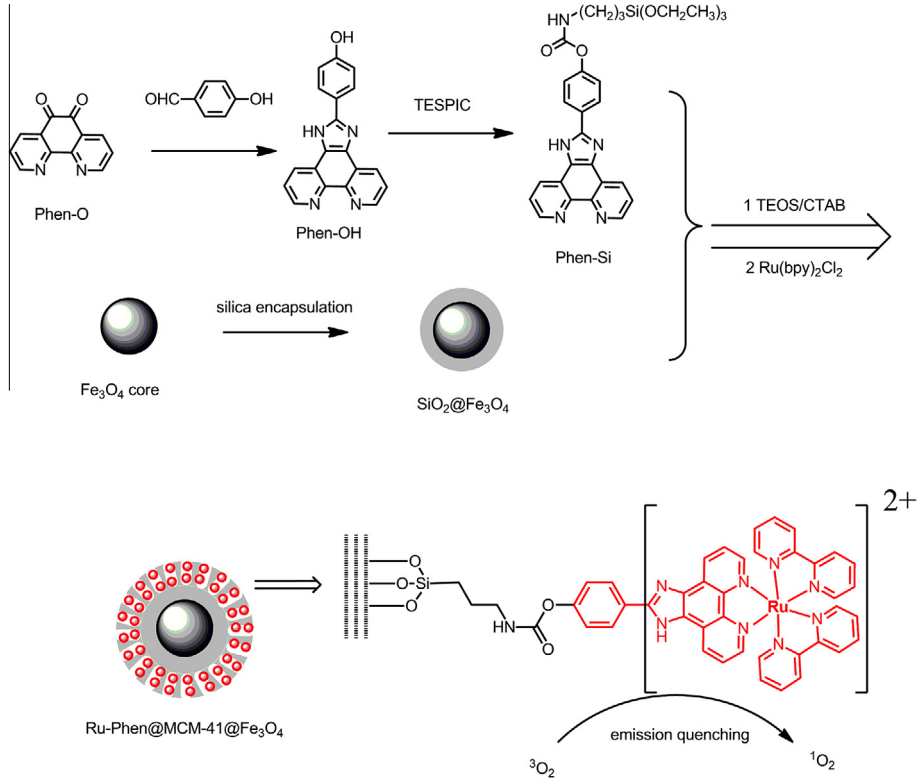

Scheme 1. Design strategy and detailed construction route of Ru-Phen@MCM-41@Fe_3O_4.

2. Experimental

2.1. General information for reagents and equipments

Starting chemicals for synthesis are summarized below. Common compounds, such as 2,2′-bipyridine (bpy, AR), 1,10-phenanthroline (Phen, AR), 4-hydroxybenzaldehyde, tetraethoxysilane (TEOS, AR), 3-(triethoxysilyl) propylisocyanate (TESPIC, AR), odium dodecyl sulfate (SDS, AR) and cetyltrimethylammonium bromide (CTAB, AR), were commercially supplied by Yongxing Chemicals and Reagents Company (Hebei, China) and used with no further purifications. Inorganic reagents and organic solvents, such as $RuCl_3{\cdot}nH_2O$ (AR), NH_4AC, $FeCl_3$ (AR), HAc, concentrated ammonia, concentrated HCl, CH_2Cl_2, $CHCl_3$, *n*-hexane, dimethyl formamide (DMF), ethanol, glycol, were commercially supplied by Yongjia Chemicals and Reagents Company (Hebei, China). Organic solvents were purified through standard procedures before use. Solvent water was deionized. Starting compound Phen-O was obtained following a literature method [11,12].

Equipments for characterization are summarized below. ^{1}H NMR, IR and MS spectra were recorded from a Varian INOVA 300 spectrometer, a Bruker Vertex 70 FTIR spectrometer (400–4000 cm^{-1}, KBr pellet technique) and a Agilent 1100 MS series/AXIMA CFR MALDI/TOF MS spectrometer, respectively. A Vario Element analyzer was used to finish elemental analysis. Emission spectra and lifetime were obtained from a Hitachi F-4500 fluorescence spectrophotometer and a two-channel TEKTRONIX TDS-3052 oscilloscope excited by 355 nm light (third-harmonic-generator pump, Nd:YAG laser), respectively. XRD measurement was finished on a Rigaku D/Max-Ra X-ray diffractometer (λ = 1.5418 Å). Magnetic response was analyzed on a MPM5-XL-5 superconducting quantum interference device. Thermal degradation analysis was recorded on a Perkin-Elmer thermal analyzer. Sample morphology was taken from a Hitachi S-4800 microscope and a JEOL JEM-2010 transmission electron microscope, respectively. Mesoporous analysis was carried out on a Nova l000 analyzer with Barrett–Joyner–Halenda (BJH) model. Diffusion coefficients of N_2 and O_2 in our composite were determined by a H-Sorb 2600T Gas analyzer. For sensing performance evaluation, Ru-Phen@MCM-41@Fe_3O_4 powder was used directly and placed in a gas chamber. Pure N_2 and pure O_2 were mixed with different concentrations via gas flow controls and directly poured into a gas chamber. Sensing performance was discussed based on Ru-Phen@MCM-41@Fe_3O_4 steady emission intensity quenching.

2.2. Synthesis of Phen-Si and Ru(bpy)$_2$Cl$_2$

Silane modified ligand Phen-Si was synthesized according to a literature procedure [11,12]. Firstly, Phen-O (20 mmol), 4-hydroxybenzaldehyde (20 mmol), NH_4AC (15.4 g) and HAc (35 mL) were mixed together and heated at 100 °C. 8 h later, this solution was poured into cold water (200 mL) and extracted with CH_2Cl_2 (25 mL × 3). The obtained crude product was recrystallized in EtOH/H_2O (V:V = 1:1), giving Phen-OH as yellow bulk. Yield 79%. ^{1}H NMR ($CDCl_3$, 300 MHz) δ [ppm]: 11.60 (s, 1H), 9.12 (m, 2H), 8.98 (m, 1H), 8.59 (m, 1H), 7.71 (m, 4H), 7.50 (m, 3H). ^{13}C NMR ($CDCl_3$), δ (ppm): 110.4, 114.7, 120.1, 121.5, 123.6, 124.8, 127.5, 131.1, 134.7, 136.9, 144.3, 150.4, 152.9, 157.5. MS *m*/*z*: $[m+1]^+$ calc. for $C_{19}H_{12}N_4O$, 312.1; found, 313.2.

Then Phen-OH (10 mmol) was dispersed in TESPIC (20 mL) and exposed to ultrasonic bath for 25 min. This mixture was heated at 80 °C under N_2 protection for 3 days and then poured into cold *n*-hexane (0 °C, 200 mL). The resulting crude product was recrystallized in ethanol to give Phen-Si as pale yellow powder. Yield 21%. ^{1}H NMR (DMSO-d6, 300 MHz) δ [ppm]: 0.51–0.54 (t, 2H), 1.14–1.17 (t, 9H), 1.51–1.54 (m, 2H), 3.01–3.04 (m, 2H), 3.75–3.78 (q, 6H), 7.38 (d, 2H), 7.83–7.86 (m, 2H), 8.27–8.29 (d, 2H), 8.95 (dd, 2H), 9.09 (dd, 2H), 11.75 (NH). ^{13}C NMR ($CDCl_3$),

δ (ppm): 11.4, 14.7, 22.0, 41.3, 52.6, 114.8, 120.1, 121.4, 122.2, 123.7, 124.8, 127.7, 128.5, 130.1, 133.6, 142.5, 150.1, 151.7, 152.9, 158.5. MS *m*/*z*: $[m+1]^+$ calc. for $C_{29}H_{33}N_5O_5Si$, 559.2; found, 560.4.

$Ru(bpy)_2Cl_2$ was obtained using a literature procedure [11,12]. Below chemicals were added into a flask and heated at 110 °C for a whole day under N_2 atmosphere, including $RuCl_3{\cdot}nH_2O$ (5 mmol), bpy (11 mmol) and redistilled DMF (35 mL). Solvent was then extracted by rotary evaporation. Solid residue was dispersed in acetone (70 mL). The remaining solid sample was mixed with ethanol (100 mL) and water (100 mL) and heated at 85 °C for 5 h under N_2 atmosphere. Later, anhydrous LiCl (100 g) was added under stirring. Ethanol was extracted by rotary evaporation. The remaining solution was cooled in refrigerator for 10 h. Crude product was recrystallized in mixed solvent ethanol:water (V:V = 1:1) and dried in vacuum at 120 °C for 2 days. MS *m*/*z*: $[m]^+$ calc. for $C_{20}H_{16}N_4$-$RuCl_2$, 484.0; found, 484.4.

2.3. Construction of SiO_2@Fe_3O_4

Precursor for magnetic supporting matrix SiO_2@Fe_3O_4 was constructed following below procedure [17,18]. Glycol (15 mL), SDS (0.2 g), NaAc (1.5 g) and $FeCl_3{\cdot}6H_2O$ (0.5 g) were mixed together and stirred at room temperature for 30 min. This mixture was sealed into a Teflon reaction kettle and heated at 200 °C for 12 h. The resulting solid sample was washed with deionized water, redispersed in ethanol (40 mL) and exposed to ultrasonic bath for 30 min. During this time, deionized water (40 mL), TEOS (0.5 g) and $NH_3{\cdot}H_2O$ (2 mL) were slowly added. This mixture was allowed to react at room temperature for 6 h, giving SiO_2@Fe_3O_4.

2.4. Construction of Ru-Phen@MCM-41@Fe_3O_4 and a reference sample

Our site-specific oxygen sensing composite (Ru-Phen@MCM-41@Fe_3O_4) was constructed following below procedure. First, MCM-41 was grew onto SiO_2@Fe_3O_4 surface with TEOS and Phen-Si as silica source. SiO_2@Fe_3O_4 (0.5 g), TEOS (1.5 g), Phen-Si (0.12 g), CTAB (0.5 g), deionized water (150 mL) and $NH_3{\cdot}H_2O$ (3 mL) were mixed together and allowed to react at room temperature for 6 h. The resulting solid product was collected and stirred in ethanol (200 mL) and concentrated HCl (10 mL) for 2 days to remove template reagent CTAB. Then this product was mixed with $Ru(bpy)_2Cl_2$ (0.5 g, excess) and ethanol (50 mL), and allowed to react at 80 °C for 8 h. The final solid product was collected, washed with ethanol and dried in vacuum to give Ru-Phen@MCM-41@Fe_3O_4 as pale dark powder. Yield (0.4 g). Elemental analysis for Ru-Phen@MCM-41@Fe_3O_4, found: C, 6.28, H, 1.22, N, 1.07%.

A similar procedure was carried out except that no Phen-Si was used in this run, giving a reference sample, so that performance comparison between this reference sample and Ru-Phen@MCM-41@Fe_3O_4 could be performed.

3. Results and discussion

3.1. Morphology of Ru-Phen@MCM-41@Fe_3O_4

Scanning electron microscope (SEM) and transmission electron microscope (TEM) images of Ru-Phen@MCM-41@Fe_3O_4 are shown in Fig. 1 to get a visual understanding on its morphology. SEM images of Fe_3O_4 core and SiO_2@Fe_3O_4 are shown in Fig. 1 as well for comparison. Owing to its magnetic nature, Fe_3O_4 particles are intensively aggregated with bad dispersal. These particles are generally spherical ones with mean diameter of ~250 nm which is slightly smaller than literature values [17,18]. Their surface, however, is rather rough with multiple bulges and graves. As for SiO_2@Fe_3O_4, silica encapsulation procedure increases its diameter to ~260 nm. Its surface is obviously smoothed, but aggregation between SiO_2@Fe_3O_4 particles is still obvious, which means that this thin SiO_2 layer is effective on modifying particle surface but limited in decreasing magnetic attraction. After MCM-41 construction and probe loading procedures, diameter of Ru-Phen@MCM-41@Fe_3O_4 is finally increased to 370 nm, with smooth surface and nearly monodispersal. Its TEM image shown in Fig. 1 indicates a clear core–shell structure in it. It is thus confirmed that MCM-41 layer has successfully blocked magnetic aggregation between these particles, showing a good dispersal. MCM-41 layer thickness is determined as ~55 nm which is slightly smaller than literature values [17,18]. We assume that these short MCM-41 tunnels may favor oxygen sensing by decreasing the number of "dead-sites" which are inaccessible to O_2 diffusion, giving improved sensitivity and fast response.

3.2. Superamagnetic feature of Ru-Phen@MCM-41@Fe_3O_4

In our target structure, magnetic core is designed for site-specific aggregation. Magnetic response of Ru-Phen@MCM-41@Fe_3O_4 is thus analyzed to evaluate its potential for site-specific aggregation. That of Fe_3O_4 core is shown in Fig. 2 for comparison. It is observed that our as-synthesized Fe_3O_4 core follows superamagnetic behavior, showing no hysteresis. Such superamagnetic nature enables it either to be aggregated to a specific-site in the presence of a magnet or to be highly dispersed in the absence of external magnetic field. Saturate magnetization value of our Fe_3O_4 core is measured as 67.1 emu g^{-1}. This value is slightly lower than literature values which can be explained by the small size of our Fe_3O_4 particles [17,18]. Literatures have suggested that Fe_3O_4 particles larger than 30 nm are supposed to follow magnetic behavior instead of superamagnetic one [19]. In this work, however, superamagnetic behavior is still observed from our as-synthesized Fe_3O_4 particles even though their diameter is as wide as 250 nm. Considering the bulges and graves on their surface, we assume that each visible Fe_3O_4 particle is actually composed of sub-particles smaller than 30 nm. As for Ru-Phen@MCM-41@Fe_3O_4, silica encapsulation and MCM-41 growth decrease its saturate magnetization value to 51.3 emu g^{-1} with its superamagnetic behavior well preserved. This decreased superamagnetic behavior is still strong enough for site-specific aggregation [17,18].

3.3. XRD pattern of Ru-Phen@MCM-41@Fe_3O_4

The Fe_3O_4 core in Ru-Phen@MCM-41@Fe_3O_4 is further analyzed and confirmed by its wide angle XRD (WAXRD) pattern, as shown in Fig. 3A. That of our as-synthesized Fe_3O_4 particles is shown for comparison. Six well-resolved diffraction peaks are observed for our as-synthesized Fe_3O_4 particles, which are indexed as (220), (311), (400), (422), (551), (440), respectively. After consulting literature reports, we come to a conclusion that Fe_3O_4 core has been successfully constructed [17,18]. Diameter of these Fe_3O_4 particles is calculated as 14.78 nm using Scherrer equation, which confirms our hypothesis that each visible Fe_3O_4 particle is actually composed of sub-particles smaller than 30 nm [17,18]. As for Ru-Phen@MCM-41@Fe_3O_4, these six diffraction peaks are still observed, which means that the Fe_3O_4 core has been well preserved after a sires procedures of silica encapsulation, MCM-41 growth and probe loading. On the other hand, their diffraction intensity is slightly decreased, which should be explained by the fact that above modification procedures actually decrease regularity of Fe_3O_4 core.

For a tentative investigation on the mesoporous tunnels on Ru-Phen@MCM-41@Fe_3O_4 surface, its small angle XRD (SAXRD) pattern is measured and shown as Fig. 3B. That of a reference sample is shown for comparison. The reference sample exhibits a sharp

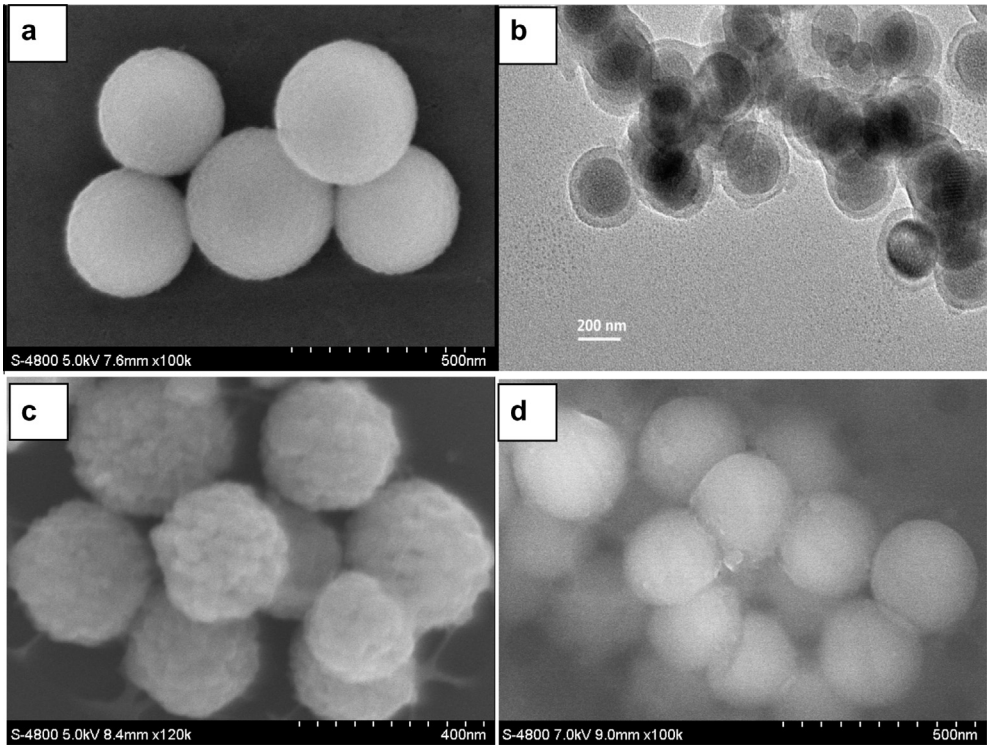

Fig. 1. SEM (a) and TEM (b) images of Ru-Phen@MCM-41@Fe_3O_4, along with SEM images of Fe_3O_4 core (c) and SiO_2@Fe_3O_4 (d).

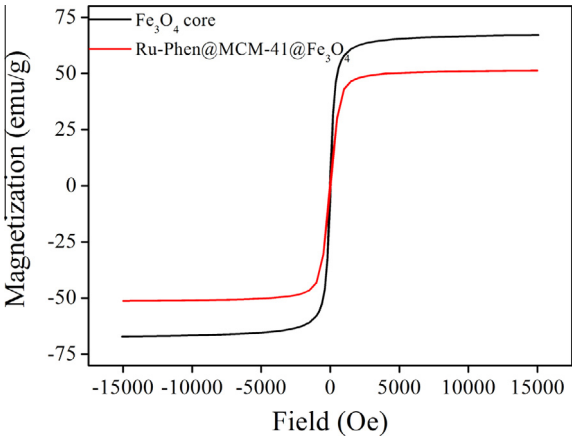

Fig. 2. Magnetic response of Ru-Phen@MCM-41@Fe_3O_4 and Fe_3O_4 core.

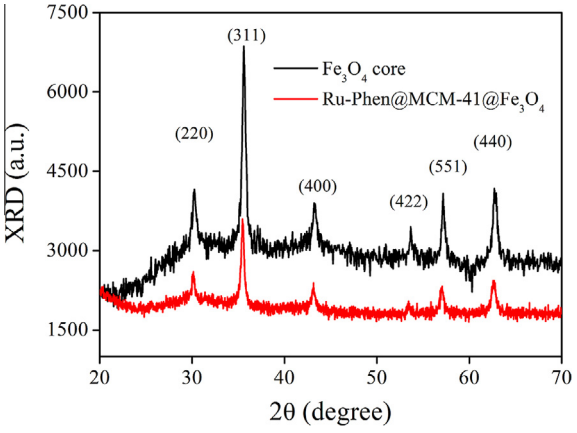

Fig. 3A. WAXRD patterns of Ru-Phen@MCM-41@Fe_3O_4 and Fe_3O_4 core.

Bragg reflection peak and two obvious shoulder peaks indexed as (100), (110) and (200) which are quite similar to those of standard MCM-41 samples [11,12]. As for Ru-Phen@MCM-41@Fe_3O_4, there are three similar peaks, suggesting that there are highly ordered hexagonal tunnels on Ru-Phen@MCM-41@Fe_3O_4 surface. On the other hand, these peaks become wider and weaker than those of the reference sample. It seems that the existence of silane coupling ligand and its Ru(II) complex in Ru-Phen@MCM-41@Fe_3O_4 slightly decreases regularity of this mesoporous structure.

3.4. N_2 adsorption/desorption measurement of Ru-Phen@MCM-41@Fe_3O_4

To further confirm the mesoporous tunnels on Ru-Phen@MCM-41@Fe_3O_4 surface, its N_2 adsorption/desorption isotherms are

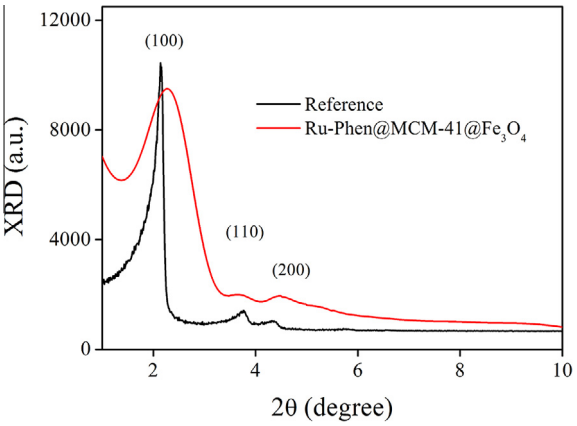

Fig. 3B. SAXRD patterns of Ru-Phen@MCM-41@Fe_3O_4 and a reference sample.

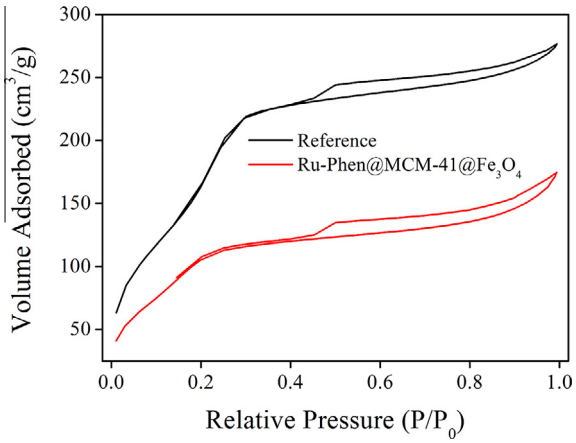

Fig. 4. N_2 adsorption/desorption isotherms of Ru-Phen@MCM-41@Fe_3O_4 and a reference sample.

shown in Fig. 4. Those of a reference sample are shown for comparison. It is observed that the two samples have nearly identical isotherms which are quite similar to those of standard MCM-41 samples [11,12]. These type IV isotherms suggest that hexangular tunnels have been successfully constructed on Ru-Phen@MCM-41@Fe_3O_4 surface and well preserved after loading probe molecules. Mesoporous parameters, including pore diameter, surface area and pore volume, are determined as 2.05 nm, 317.18 $m^2\ g^{-1}$ and 0.206 $cm^3\ g^{-1}$, respectively, for Ru-Phen@MCM-41@Fe_3O_4. Corresponding values of the reference sample containing no probe are 2.74 nm, 713.64 $m^2\ g^{-1}$ and 0.389 $cm^3\ g^{-1}$, respectively. It is obvious that mesoporous parameters are all decreased in Ru-Phen@MCM-41@Fe_3O_4 after loading probe molecules, which tentatively confirms that our Ru(II)-based probe has been successfully immobilized in MCM-41 tunnels.

3.5. IR spectrum and thermogravimetry analysis of Ru-Phen@MCM-41@Fe_3O_4

Aiming at a confirmation on the covalent immobilization of probe in Ru-Phen@MCM-41@Fe_3O_4, IR spectra of Phen-Si and Ru-Phen@MCM-41@Fe_3O_4 are shown in Fig. 5. That of a reference sample is shown for comparison. The reference sample containing no probe demonstrates only a few characteristic bands peaking at 458 cm^{-1}, 583 cm^{-1}, 802 cm^{-1} and 1637 cm^{-1}, respectively. The first one is attributed to vibration of Si–O–Si framework. The latter three ones belong to plane blending and stretching vibrations from Si–O bonds. These characteristic bands are consistent with silica shell and MCM-41 layer on this reference sample. As for Phen-Si, plane blending and stretching vibrations from Si–O bonds (583 cm^{-1}, 802 cm^{-1} and 1637 cm^{-1}) are observed from its IR spectrum, without vibration of Si–O–Si framework. The sharp bands peaking at 1543 cm^{-1} and 1700 cm^{-1} belong to vibrations of –Si–O–C group. A group of bands around 2973 cm^{-1} are assigned to stretching vibrations of $-(-CH_2-)_3-$ group [11,12]. Above bands are consistent with Phen-Si molecular structure. As for the IR spectrum of Ru-Phen@MCM-41@Fe_3O_4, characteristic bands from Si–O–Si framework and Si–O bonds (458 cm^{-1}, 583 cm^{-1}, 802 cm^{-1} and 1637 cm^{-1}) are clearly observed. Stretching vibration of $-(-CH_2-)_3-$ group (2931 cm^{-1}) exhibits blue shift tendency compared to that of Phen-Si, which should be attributed to the covalent grafting with silica backbone. Vibrations of –Si–O–C group (1543 cm^{-1} and 1700 cm^{-1}) are completely missing, owing to Phen-Si hydrolysis. Taking above result into account, it is safe to say that our Ru(II)-based probe has been covalently immobilized in Ru-Phen@MCM-41@Fe_3O_4 through our silane coupling ligand, serving as sensing probe.

To get a tentative understanding on probe loading content in Ru-Phen@MCM-41@Fe_3O_4, its thermogravimetry analysis (TGA) and derivative thermogravimetry (DTG) plots are shown in Fig. 6. It is observed that Ru-Phen@MCM-41@Fe_3O_4 is quite stable below 200 °C, showing no obvious weight loss. It is thus confirmed that this composite is thermally stable enough for normal applications. Upon even higher temperatures, there are two major weight loss regions, ranging from 200 °C to 340 °C and from 407 °C to 522 °C, respectively. The first weight loss region is responsible for 11.4 wt% weight loss with multiple endothermic peaks around 240 °C. Combined with TGA curve of a similar Ru(II) complex $[Ru(bpy)_2(Phen\text{-}OH)]Cl_2$ (Fig. S1, Supporting information), this region is attributed to the thermal release of Ru(II)-probe. In other words, probe loading content in Ru-Phen@MCM-41@Fe_3O_4 is as high as 11.4 wt%. This value is slightly higher than literature values, given our short MCM-41 tunnels [17,18]. It seems that these short tunnels are more efficient on loading probe than long ones do. The last weight loss region causes 6.9 wt% weight loss with an endothermic peak of 441 °C. We attribute this region to the thermal degradation of organosilicate framework in Ru-Phen@MCM-41@Fe_3O_4.

3.6. Performance evaluation of site-specific O_2 sensing

3.6.1. Site-specific aggregation

Site-specific aggregation of Ru-Phen@MCM-41@Fe_3O_4 should be firstly evaluated since it is our primary objective. In virtue of

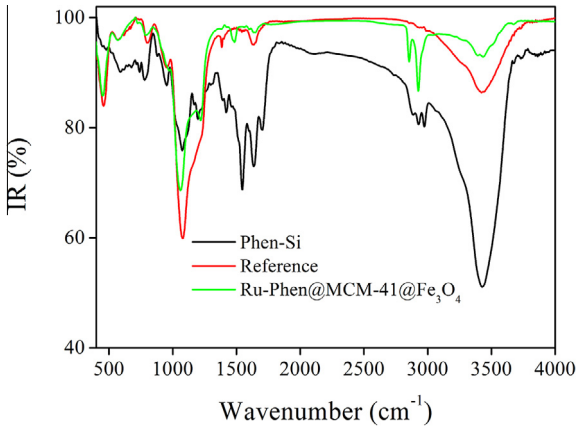

Fig. 5. IR spectra of Ru-Phen@MCM-41@Fe_3O_4, Phen-Si and a reference sample.

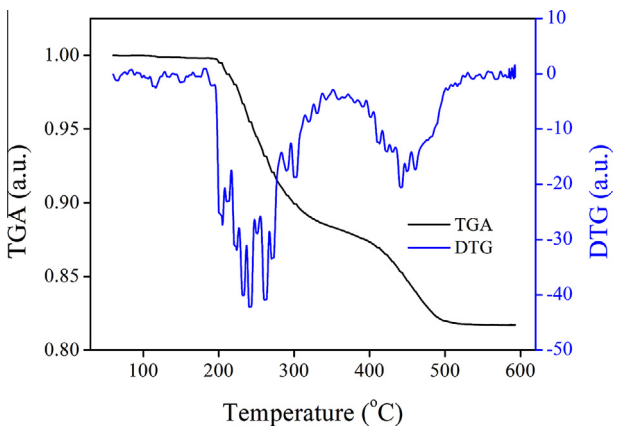

Fig. 6. TGA and DTG analysis of Ru-Phen@MCM-41@Fe_3O_4.

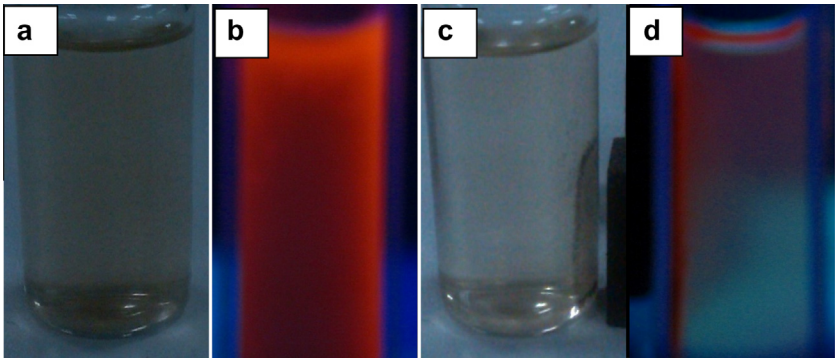

Fig. 7. Photos of Ru-Phen@MCM-41@Fe_3O_4 turbid liquid in ethanol ((a) no magnet, no UV; (b) no magnet, UV 365 nm; (c) magnet, no UV; (d) magnet, UV 365 nm).

its hydrophilic silica shell, this composite can be readily dispersed in aqueous solution when there is no external magnetic field, as shown in Fig. 7. Upon photoexcitation of 365 nm, uniform red emission is observed from the whole turbid liquid, which is consistent with MLCT emission of Ru(II) complexes [11,12]. On the other hand, owing to its superamagnetic nature, Ru-Phen@MCM-41@Fe_3O_4 can be readily aggregated to a specific site by a magnet. Correspondingly, its red emission is concentrated at this site. We come to a conclusion that our Ru(II)-based probe has been uniformly immobilized and well preserved in MCM-41 matrix, which is positive for linear oxygen sensing. It is thus safe to say that our primary objective of site-specific aggregation has been achieved.

3.6.2. Sensing sensitivity

By recording spectral response of Ru-Phen@MCM-41@Fe_3O_4 emission under various O_2 concentrations ranging from 0% to 100%, its oxygen sensing performance can be evaluated. As shown in Fig. 8, Ru-Phen@MCM-41@Fe_3O_4 has a broad emission band under pure N_2 condition peaking at 591 nm with FWHM of 78 nm which is consistent with its red emission shown in Fig. 7. Here, FWHM means full width at half maximum. No vibronic progressions are found, suggesting that corresponding emissive center has a charge transfer character. This finding is consistent with the MLCT emissive nature of Ru(II) complex. Emission intensity of Ru-Phen@MCM-41@Fe_3O_4 gradually decreases with increasing O_2 concentrations with band shape well preserved, which means that its emissive center does not change. It is hereby confirmed that Ru-Phen@MCM-41@Fe_3O_4 emission is quenchable by O_2, making itself an oxygen sensing material.

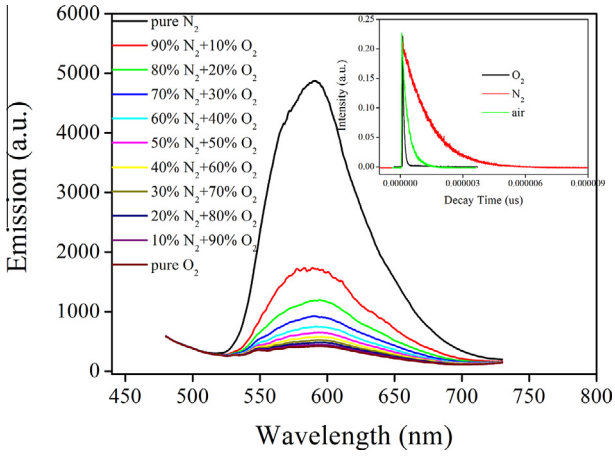

Fig. 8. Spectral response of Ru-Phen@MCM-41@Fe_3O_4 emission under various O_2 concentrations ranging from 0% to 100% with interval of 10%. Inset: emission decay dynamics of Ru-Phen@MCM-41@Fe_3O_4 under pure N_2 and pure O_2 conditions.

To evaluate its sensing performance, maximum sensitivity is defined as the value of I_0/I_{100}, according to a literature quotation. Here I_0 stands for emission intensity in the absence of O_2 and I_{100} is that in pure O_2, respectively [11,12]. Maximum sensitivity of Ru-Phen@MCM-41@Fe_3O_4 is calculated as 11.5 which is much higher than literature values (~5) of similar magnetic-mesoporous sensing composite samples [20–23]. We attribute this good sensitivity to the following factors. (1) There are large coplanar conjugation planes in our Ru(II) complex which may increase electronic distribution and lifetime of probe excited electrons. Correspondingly, sensing collision probability between excited probe and analyte should be increased. (2) O_2 molecules are efficiently transported in MCM-41 tunnels with high diffusion coefficient, favoring oxygen sensing.

3.6.3. Dynamic sensing mechanism and working plot

To get a further understanding on the energy transfer between our probe and O_2 molecules and then specify its sensing mechanism, emission decay dynamics of Ru-Phen@MCM-41@Fe_3O_4 under pure N_2 and pure O_2 conditions are recorded and shown as the inset of Fig. 8. It is observed that both emission decay curves follow single exponential decay pattern. In the absence of O_2, its lifetime is as long as 1.30 μs, indicating the phosphorescent nature of this emission. This long-lived emissive center is consistent with triplet MLCT emissive center of Ru(II) complexes, further confirming that this emission comes from Ru(II)-based probe [11,12]. Its single exponential decay pattern confirms that these probe molecules are homogeneously immobilized in supporting matrix, which is consistent with our observation from Fig. 7. In the presence of O_2, Ru-Phen@MCM-41@Fe_3O_4 emission lifetime is greatly decreased to 0.06 μs under pure O_2 condition and 0.29 μs under air condition, respectively, suggesting that its emissive center is quenched by O_2 molecules. We thus come to a conclusion that Ru-Phen@MCM-41@Fe_3O_4 emissive center is directly quenched by O_2 molecules through collision-induced energy transfer. This procedure falls in the definition of a dynamic quenching mechanism, as described by Formula 1. Here "*" means an excited state.

$$\text{Ru(II)-probe}^* + {}^3O_2 \rightarrow \text{Ru(II)-probe} + {}^1O_2^* \quad (1)$$

Above analysis has confirmed that: (1) all probe molecules are homogeneously distributed in supporting matrix; (2) probe emission follows single exponential decay pattern; (3) probe excited state is quenched by a dynamic energy transfer. In this case, probe emission intensity variation upon various analyte concentrations can be expressed by Stern–Volmer equation, as shown by Formula 2 [11,12]. Here I and I_0 stand for emission intensity and that in pure N_2 atmosphere, respectively. K_{SV} and $[O_2]$ are Stern–Volmer constant and O_2 concentration, respectively. According to Formula 2, an ideal plot of I_0/I against $[O_2]$ is supposed to be a linear curve with slope of K_{SV}. The I_0/I versus $[O_2]$ plot of Ru-Phen@MCM-41@Fe_3O_4

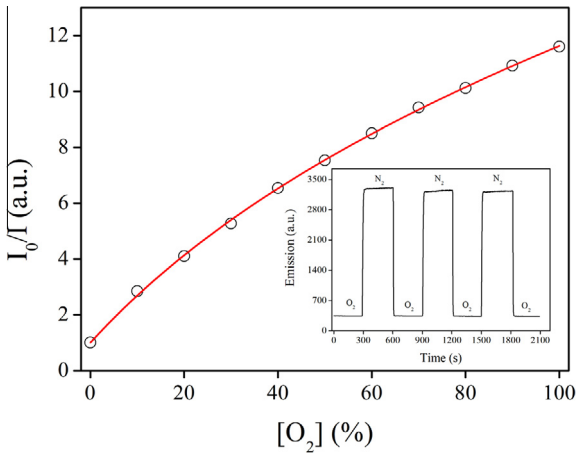

Fig. 9. Stern–Volmer working plot of Ru-Phen@MCM-41@Fe_3O_4 emission under various O_2 concentrations ranging from 0% to 100% with interval of 10%. Inset: emission intensity monitoring of Ru-Phen@MCM-41@Fe_3O_4 upon periodically changing environment atmosphere between 100% N_2 and 100% O_2.

is close to a linear one, as shown in Fig. 9. However, a more comprehensive model should be proposed to perfectly explain this sensing plot.

$$I_0/I = 1 + K_{SV}[O_2] \quad (2)$$

Considering that there may be "dead-sites" in Ru-Phen@MCM-41@Fe_3O_4 which are inaccessible to O_2 diffusion, it is rational to assume that there are two or more kinds of sensing sites. Only one of them is sensitive to and quenchable by O_2 molecules, while the others are not. In this case, sensing contribution of each site should be taken into account. A modified two-site model is then proposed to describe this case, as shown by Formula 3. Here f_1 and f_2 stand for fractional contributions of sensing sites ($f_1 + f_2 = 1$), K_{SV1} and K_{SV2} mean Stern–Volmer quenching constants of these sensing sites, respectively [11,12]. This modified two-site model can well describe our working plot, as shown in Fig. 9, with $f_1 = 0.953$, $f_2 = 0.047$, $K_{SV1} = 0.1917$ $[O_2\%]^{-1}$ and $K_{SV2} = 0.0022$ $[O_2\%]^{-1}$ ($R^2 = 0.999$), respectively. It is observed that K_{SV2} is greatly smaller than K_{SV1} by two orders of magnitude, indicating that site-2 is nearly immune to O_2 molecules. If we set K_{SV2} as 0, then Formula 3 can be further simplified, with $f_1 = 0.964$, $f_2 = 0.036$, and $K_{SV1} = 0.1800$ $[O_2\%]^{-1}$ ($R^2 = 0.999$), respectively. This simplified model can well fit our working plot. Maximum sensitivity and linearity of working plot are compromised by site-2, even though its contribution is slim. Site-2 is attributed to the "dead-sites" in Ru-Phen@MCM-41@Fe_3O_4 which are inaccessible to O_2 diffusion. Its slim contribution suggests that most MCM-41 tunnels can efficiently transport O_2 molecules, as anticipated in Section 3.2. For performance improvement, such "dead-sites" should be eliminated so that a more linear working plot can be expected.

$$\frac{I_0}{I} = \frac{1}{\frac{f_1}{1+K_{SV1}pO_2} + \frac{f_2}{1+K_{SV2}pO_2}} \quad (3)$$

3.6.4. Response/recovery character and photostability

Aiming at a further confirmation on the dependence between emission quenching and O_2 presence, surrounding environment is periodically changed between pure O_2 and pure N_2 when Ru-Phen@MCM-41@Fe_3O_4 emission is continuously monitored. As shown by the inset of Fig. 9, sample emission is clearly dependent on O_2 presence. Under pure O_2 condition, sample emission is decreased to minimal level and maintained, showing sensing signal. When atmosphere is switched to pure N_2 condition, emission is quickly recovered to normal level. After a few such cycles, maximum emission can always be recovered, indicating that Ru-Phen@MCM-41@Fe_3O_4 has a good photostability owing to the covalent grafting between probe and supporting matrix.

For discussion convenience, we define response time as the time taken by Ru-Phen@MCM-41@Fe_3O_4 to decrease to 5% of its emission maximum when surrounding environment is switched from pure N_2 to pure O_2 [11,12]. Similarly, recovery time is defined as the time taken by Ru-Phen@MCM-41@Fe_3O_4 to increase to 95% of its emission maximum when surrounding environment is switched from pure O_2 to pure N_2. Response time of Ru-Phen@MCM-41@Fe_3O_4 is calculated as 10 s which is comparable to or even shorter than literature values (12–21 s) of similar magnetic-mesoporous sensing composite samples [20–23]. The following factors should be blamed responsible. (1) The large coplanar conjugation planes in probe increase electronic distribution and lifetime of probe excited electrons. By offering more sensing collision chances, excited probe can be efficiently quenched. (2) Supporting matrix provides highly ordered tunnels with high diffusion coefficient, guaranteeing efficient oxygen sensing. On the other hand, recovery time is calculated as 30 s and found much longer than response time. This phenomenon has been blamed to diffusion-controlled dynamic response and recovery behavior [24]. Diffusion coefficients of N_2 and O_2 in our composite are measured as 0.61×10^{-8} m^2/s and 1.72×10^{-8} m^2/s, respectively. This result is consistent with our observation that recovery time is longer than response time. Mills and coworkers have reported that response time and recovery time can be calculated by Formulas 4 and 5, which mathematically explains why a recovery time (T_{rec}) is always longer than a response time (T_{res}) [25]. Here, b is sample thickness, D is diffusion coefficient, K_{SV} is Stern–Volmer constant, respectively.

$$T_{res} = 3.06\left(\frac{b^2}{D}\right)\mathrm{Ln}\left[10 - \frac{9K_{SV}\{PO_2(final) - PO_2(initial)\}}{1 + PO_2(final)K_{SV}}\right] \quad (4)$$

$$T_{rec} = 3.06\left(\frac{b^2}{D}\right)\mathrm{Ln}\left[10 + \frac{9K_{SV}\{PO_2(final) - PO_2(initial)\}}{1 + PO_2(final)K_{SV}}\right]. \quad (5)$$

3.6.5. Selectivity: interfering effect from other gases

For a tentative evaluation on selectivity of Ru-Phen@MCM-41@Fe_3O_4 towards O_2, its emission spectra under pure N_2, CO_2 and a few VOC gases, including benzene, toluene, $CHCl_3$ and CH_2Cl_2 vapors, are shown in Fig. 10. No obvious interfering effect is

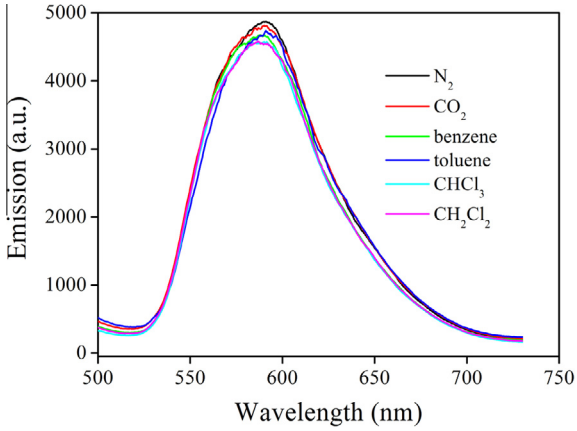

Fig. 10. Emission spectra of Ru-Phen@MCM-41@Fe_3O_4 under the following conditions: N_2 (101 kPa), CO_2 (101 kPa), benzene (13.33 kPa), toluene (4.89 kPa), $CHCl_3$ (21.2 kPa) and CH_2Cl_2 (46.5 kPa).

observed for CO_2. This is because CO_2 has a closed-shell structure and is not open for energy transfer from excited Ru(II) center [11,12]. The presence of benzene and toluene vapors, however, tends to quench Ru-Phen@MCM-41@Fe_3O_4 emission. It is assumed that the conjugation chain in these organic molecules may capture excited electrons and thus quench Ru-Phen@MCM-41@Fe_3O_4 emission. As for $CHCl_3$ and CH_2Cl_2 vapors, they may quench Ru-Phen@MCM-41@Fe_3O_4 emission by coordinating with excited Ru(II) center. For performance improvement, selectivity of our sensing probe should be taken into account.

4. Conclusion

As a conclusion, we designed and constructed an oxygen sensing composite with site-specific aggregation feature. Fe_3O_4 core coated with silica molecular sieve MCM-41 was used supporting matrix. A Ru(II)-based probe was covalently immobilized into this supporting matrix through a silane coupling ligand. This composite structure was analyzed and discussed by means of SEM, TEM, XRD, IR, TGA and N_2 adsorption/desorption. Photophysical analysis of this composite under various O_2 concentrations suggested that its emission was quenchable by O_2 with good stability through a dynamic mechanism. Sensitivity of 11.5 and short response time of 10 s were obtained. This good performance was attributed to the following factors: (1) the large coplanar conjugation planes in probe increased electronic distribution and lifetime of probe excited electrons. By offering more sensing collision chances, excited probe could be efficiently quenched. (2) supporting matrix provided the highly ordered tunnels with high diffusion coefficient, guaranteeing efficient oxygen sensing. On the other hand, linearity of our working plot was yet to be satisfied. "Dead-sites" should be eliminated so that a linear working plot can be expected.

Acknowledgment

The authors gratefully thank our university for the equipments and financial support.

Appendix A. Supplementary material

Supplementary data associated with this article can be found, in the online version, at http://dx.doi.org/10.1016/j.ica.2016.02.061.

References

[1] Y. Guo, L. Zhang, S. Zhang, Y. Yang, X. Chen, M. Zhang, Biosens. Bioelectron. 63 (2015) 61.
[2] D. Sarkar, A. Pramanik, S. Jana, P. Karmakar, T.K. Mondal, Sens. Actuators, B 209 (2015) 138.
[3] O.S. Wolfbeis, Anal. Chem. 80 (2008) 4269.
[4] C. Baleizao, S. Nagl, M. Schaferling, M.N. Berberan-Santos, O.S. Wolfbeis, Anal. Chem. 80 (2008) 6449.
[5] L.C. Clark Jr., Trans. Am. Soc. Artif. Intern. Organs 2 (1956) 41.
[6] L.W. Winkler, Ber. Dtsch. Chem. Ges. 21 (1888) 2843.
[7] M.R. Awual, M.M. Hasan, M.A. Khaleque, Sens. Actuators, B 209 (2015) 194.
[8] C.S. Chu, C.Y. Chuang, Sens. Actuators, B 209 (2015) 94.
[9] G. Zhang, J. Chen, S.J. Payne, S.E. Kooi, J.N. Demas, C.L. Fraser, J. Am. Chem. Soc. 129 (2007) 15728.
[10] A. Gulino, S. Giuffrida, P. Mineo, M. Purrazzo, E. Scamporrino, G. Ventimiglia, M.E. Van der Boom, I. Fragala, J. Phys. Chem. B 110 (2006) 16781.
[11] B. Lei, B. Li, H. Zhang, L. Zhang, W. Li, J. Phys. Chem. C 111 (2007) 11291.
[12] B. Lei, B. Li, H. Zhang, S. Lu, Z. Zheng, W. Li, Y. Wang, Adv. Funct. Mater. 16 (2006) 1883.
[13] L. Yang, J.K. Feng, A.M. Ren, M. Zhang, Y.G. Ma, X.D. Liu, Eur. J. Inorg. Chem. 10 (2005) 1867.
[14] J. Jia, Y. Tian, Z. Li, Synth. Met. 161 (2011) 1377.
[15] Z. Si, X. Li, X. Li, H. Zhang, J. Organomet. Chem. 694 (2009) 3742.
[16] L. Zhang, S. Yue, B. Li, D. Fan, Inorg. Chim. Acta 384 (2012) 225.
[17] Y. Wang, B. Li, L. Zhang, H. Song, Langmuir 29 (2013) 1273.
[18] Y. Wang, B. Li, L. Zhang, P. Li, L. Wang, J. Zhang, Langmuir 28 (2012) 1657.
[19] L. Zhang, W. Sun, P. Cheng, Molecules 8 (2003) 207.
[20] J. Li, C. Yang, Y. Wu, B. Wang, W. Sun, T. Shao, Inorg. Chim. Acta 441 (2016) 1.
[21] D. Wan, Y. Li, J. Liu, Inorg. Chim. Acta 437 (2015) 120.
[22] P. Wan, L. Wang, Inorg. Chim. Acta 436 (2015) 45.
[23] J. Li, C. Yang, Y. Wu, B. Wang, W. Sun, T. Shao, Inorg. Chim. Acta 442 (2016) 111.
[24] S.M. Kuang, D.G. Cuttell, D.R. McMillin, P.E. Fanwick, R.A. Walton, Inorg. Chem. 41 (2002) 3313.
[25] A. Mills, A. Pepre, Anal. Chem. 69 (1997) 4653.